Journal of Hazardous Materials 442 (2023) 129966

Contents lists available at ScienceDirect

Journal of Hazardous Materials

journal homepage: www.elsevier.com/locate/jhazmat

Low-temperature persulfate activation by powdered activated carbon for simultaneous destruction of perfluorinated carboxylic acids and 1,4-dioxane

Katherine E. Manz [a], Indrek Kulaots [a], Caroline A. Greenley [a], Patrick J. Landry [b], K.V. Lakshmi [b], Matthew J. Woodcock [a], Lucas Hellerich [c], J. Daniel Bryant [d], Mike Apfelbaum [e], Kurt D. Pennell [a,*]

[a] School of Engineering, Brown University, Providence, RI 02912, USA
[b] Department of Chemistry and Chemical Biology and The Baruch '60 Center for Biochemical Solar Energy Research, Rensselaer Polytechnic Institute, Troy, NY 12180, USA
[c] Woodard & Curran, 213 Court Street, 4th Floor, Middletown, CT 06457, USA
[d] Woodard & Curran, 50 Millstone Road, Building 400, East Windsor, NJ 08520, USA
[e] Woodard & Curran, 40 Shattuck Road, Suite 110, Andover, MA 01810, USA

HIGHLIGHTS

- Persulfate is activated by powder activated carbon (PAC) at temperatures less than 25 °C.
- Co-contaminants 1,4-dioxane and perfluorooctanoic acid are degraded at relevant temperatures.
- Targeted and non-targeted mass spectrometry are used to establish PFOA degradation mechanism.

GRAPHICAL ABSTRACT

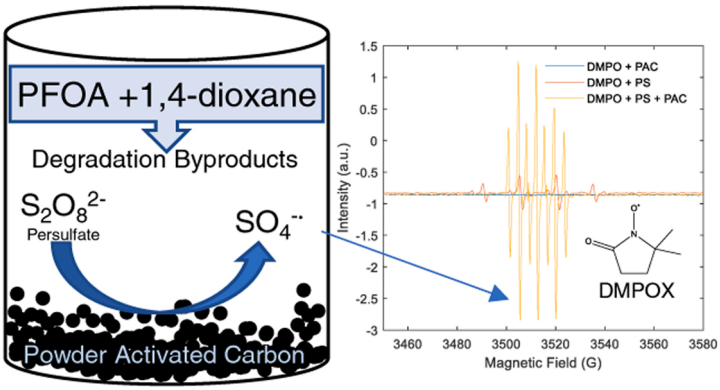

ARTICLE INFO

Editor: <Lee Blaney>

Keywords:
Persulfate
Powdered activated carbon (PAC)
Perfluorooctanoic acid (PFOA)
1

ABSTRACT

Carbonaceous materials have emerged as a method of persulfate activation for remediation. In this study, persulfate activation using powdered activated carbon (PAC) was demonstrated at temperatures relevant to groundwater (5–25 °C). At room temperature, increasing doses of PAC (1–20 g L^{-1}) led to increased persulfate activation ($3.06 \times 10^{-6} s^{-1}$ to 2.10×10^{-4} with 1 and 20 g L^{-1} PAC). Activation slowed at lower temperatures (5 and 11 °C); however, substantial (>70 %) persulfate activation was achieved. PAC characterization showed that persulfate is activated at the surface of the PAC, as indicated by an increase in the PAC C:O ratio. Similarly,

Abbreviations: ISCO, in situ chemical oxidation; PAC, powdered activated carbon; DMPO, 5,5-dimethyl-1-pyrroline N-Oxide; PFOA, perfluorooctanoic acid.

* Corresponding author.
E-mail address: kurt_pennell@brown.edu (K.D. Pennell).

https://doi.org/10.1016/j.jhazmat.2022.129966
Received 31 May 2022; Received in revised form 8 September 2022; Accepted 9 September 2022
Available online 12 September 2022

4-dioxane
Spin trapping
DMPO radical adducts
In-situ chemical oxidation (ISCO)

electron paramagnetic resonance (EPR) spectroscopy studies with a spin trapping agents (5,5-dimethyl-1-pyrroline N-oxide (DMPO)) and 2,2,6,6-tetramethylpiperidine (TEMP) revealed that singlet oxygen was not the main oxidizing species in the reaction. DMPO was oxidized to form 5,5-dimethylpyrrolidone-2(2)-oxyl-(1) (DMPOX), which forms in the presence of strong oxidizers, such as sulfate radicals. The persulfate/PAC system is demonstrated to simultaneously degrade both perfluorooctanoic acid (PFOA) and 1,4-dioxane at room temperature and 11 °C. With a 20 g L^{-1} PAC and 75 mM persulfate, 80 % and 70 % of the PFOA and 1,4-dioxane, respectively, degraded within 6 h at room temperature. At 11 °C, the same PAC and persulfate doses led to 57% dioxane degradation and 54 % PFOA degradation within 6 h. Coupling PAC with persulfate offers an effective, low-cost treatment for simultaneous destruction of 1,4-dioxane and PFOA.

1. Introduction

Persulfate oxidation chemistry, which can be applied as either *in* or *ex situ* remediation technology, has become an increasingly common for the treatment of contaminated soil and groundwater. Persulfate has an oxidation potential of 2.01 V. Upon activation, persulfate produces reactive oxygen species (ROS) with even higher oxidation potential, which react non-selectively with groundwater contaminants (Manz and Carter, 2017, 2018; Matzek and Carter, 2016; Tsitonaki et al., 2010). Activation of persulfate ($S_2O_8^{2-}$) can be achieved using external energy from sources including heat, UV light irradiation, microwave, chemical reaction (with transition metals such as iron or alkaline pH adjustment) (Furman et al., 2010; Matzek and Carter, 2016; Mitchell et al., 2014). The primary ROS produced by persulfate is the sulfate ($SO_4^{\cdot-}$) radical (E^0 = 2.6 V) (**Reaction 1**) (Kolthoff and Miller, 1951). Activation techniques that utilize energy, such as heat and UV light, form two sulfate radicals (**Reaction 1**), through cleavage of the peroxide bond in the persulfate anion. Activation techniques that rely on an electron donor, such as a transition metal, generate a single sulfate radical (**Reaction 1**) through an oxidation-reduction reaction. Secondary radicals propagate from sulfate radical reactions, including the reaction with water to form the hydroxyl ($OH^{\cdot}$) (E^0 = 2.8 V) radicals (**Reaction 2**). *In-situ* chemical oxidation (ISCO) using persulfate activated by chemical reaction has become more widespread; however, maintaining the activator in the subsurface is critical for in-situ implementation.

$$S_2O_8^{2-} + activator \rightarrow \quad SO_4^{\cdot-} + \quad \left(SO_4^{\cdot-} \quad or \quad SO_4^{2-}\right) \tag{1}$$

$$SO_4^{\cdot-} + \quad H_2O \rightarrow \quad OH^{\cdot} + \quad H^+ + SO_4^{2-} \tag{2}$$

Carbon-based materials are ideal persulfate activators for application in situ because they do not change form with pH change and have high surface areas. A variety of carbon materials, including biochar, carbon nanotubes, activated carbon (AC), granular activated carbon (GAC), and carbon materials doped with heteroatoms, have been shown to yield persulfate activation at 25 °C (Fang et al., 2015; Huang et al., 2021; Lee et al., 2015, 2020; Liu et al., 2022b). Activated carbons, including colloidal, powder and granular forms, are of particular interest for use as an in-situ persulfate activator because they can be used to create permeable adsorptive barriers (PABs) for contaminant retention of groundwater contaminants, such as per- and polyfluorinated alkyl substances (PFAS) (Annamalai et al., 2022; Coyle et al., 2021; Liu et al., 2022a, 2020a; Masud et al., 2022; McGregor, 2018, 2020; Septian et al., 2021). In PABs, colloidal activated carbon and PAC are injected for groundwater remediation under pressure; the particles do not transport substantial distances (e.g., < 1 m) and thereby creates a zone of porous media containing AC which adsorbs the contaminants without reducing the permeability of the native porous medium (Liu, 2020a). Thus, by combining persulfate and an absorptive technology, the permeable barrier could provide both adsorption and reactive transformation of groundwater contaminants to establish a permeable reactive barrier (PRB).

The mechanism of persulfate activation using activated carbons has not been established in the literature due in large part to the complicated nature of the reaction (Duan et al., 2017). Both radical and non-radical pathways have been proposed (Lee et al., 2013, 2022; Yang et al., 2011; Yao et al., 2019). In radical pathways, sulfate radicals are thought to form through electron conduction and then further react with water to form hydroxyl and/or superoxide ($O_2^{\cdot-}$) radicals, or to form radicals at the surface of the PAC (**Reactions 3 and 4**, respectively) (Huang et al., 2021; Liang et al., 2009). In non-radical forming pathways, it is thought that surface electron transfer occurs, an activated complex forms at the surface of the carbon material, or singlet oxygen is generated (Huang et al., 2021; Yao et al., 2019). Many studies have utilized radical quenching experiments that employ radical scavengers, such as methanol and tert-butyl alcohol, to determine whether the reaction is radical or non-radical forming (Forouzesh et al., 2019; Huang et al., 2021; Yang et al., 2011; Zhang et al., 2021a). Interpretation of these experiments can be difficult with carbon-based activation because of adsorption. Thus, radical quenching experiments have led some researchers to suggest the involvement of radicals, while leading others to suggest a non-radical forming mechanism (Duan et al., 2016; Yang et al., 2011).

$$GACsurface - OOH + \quad S_2O_8^{2-} \rightarrow \quad SO_4^{\cdot-} + GACsurface - OO^{\cdot} + HSO_4^- \tag{3}$$

$$GACsurface - OOH + \quad S_2O_8^{2-} \rightarrow \quad SO_4^{\cdot-} + GACsurface - O^{\cdot} + HSO_4^- \tag{4}$$

Nevertheless, carbon and persulfate based PRBs offer a relatively low-cost, in-situ technology for remediation of persistent chemicals, such as per- and polyfluorinated alkyl substances (PFAS). The occurrence of PFAS, including perfluorooctanoic acid (PFOA), was significantly correlated with 1,4-dioxane in data collected from US public drinking water supplies as a part of third round of the Unregulated Contaminant Monitoring Rule (Adamson et al., 2017). Thus, PFOA and 1,4-dioxane are common co-contaminants in groundwater (Suthersan et al., 2016). PFOA and 1,4-dioxane have clean-up guidance that ranges from 1 to more than 1000 ng L^{-1} (Abunada et al., 2020; Li et al., 2010; McElroy et al., 2019; Simon et al., 2019). Although ACs provide high sorption capacity for longer chain PFAS (Liu et al., 2020a; McCleaf et al., 2017). However, adsorption is ineffective for 1,4-dioxane removal due to its low adsorption capacity to carbon (McElroy et al., 2019). It has been observed that 1,4-dioxane is readily oxidized by unactivated persulfate, $SO_4^{\cdot-}$, and $HO^{\cdot}$ (Cashman et al., 2019; Evans et al., 2019; Kambhu et al., 2017; Zhao et al., 2014), while PFOA oxidation requires the generation of sulfate radicals (Bruton and Sedlak, 2017; Lee et al., 2012a, 2012b; Shojaei et al., 2021). Previous studies have reported that persulfate can oxidize organic contaminants, including PFOA, in the presence of activated carbon (AC) (Lee et al., 2020, 2013; Sun et al., 2016; Yao et al., 2019). However, temperatures representative of actual groundwater conditions have yet to be studied (most experiments have been performed at ≥20 °C).

Activation of persulfate by AC at ambient temperature presents the potential for soil and groundwater remediation of contaminant mixtures with a range of susceptibilities to oxidative and sorptive treatment. This technology may be applied in-situ to contaminated groundwater as a PRB, which could offer a cost-effective remediation strategy in comparison with *ex situ* treatment, which requires extraction, treatment with multiple energy-intensive processes, and the management of secondary waste streams such as spent carbon. Understanding the mechanism of

persulfate activation using powdered AC (PAC) and its effectiveness at low temperatures is essential for in-situ application of PAC and persulfate. In the present study, we performed lab-scale batch studies at 5, 11 and 22 °C to understand persulfate activation. We then characterized the PAC before and after activation using fourier-transform infrared spectroscopy (FTIR), X-ray photoelectron spectroscopy (XPS), Brunauer-Emmett-Teller (BET) surface area, and thermogravimetric analysis (TGA) and employed EPR spectroscopy to investigate the activation of persulfate by PAC and radical formation. Finally, we demonstrate the efficacy of the PAC-persulfate system for simultaneous degradation of PFOA and 1,4-dioxane.

2. Materials and methods

2.1. Chemicals and reagents

All solutions were prepared using water purified by a Millipore Milli-Q® Reference purification system (18.2 MΩ.cm at 25 °C and total organic content below 5 ppb). Inorganic salts were purchased from Fisher Scientific (Waltham, MA, USA) (Total Ionic Strength Adjustment Buffer (TISAB), 10 ppm fluoride with TISAB standard, and anhydrous potassium persulfate, sodium bicarbonate, magnesium sulfate, sodium chloride, and calcium chloride); except for potassium iodide (99%) and potassium chloride, which were purchased from Alpha Aesar and Macron Fine chemicals, respectively. Darco® PAC (100 mesh) was purchased from Millipore Sigma (Burlington, MA, USA). 1,4-dioxane (99.8% extra dry) and perfluorooctanoic acid (PFOA) (96%), were purchased from Acros Organics and Sigma Millipore, respectively. Mass spectrometry analysis revealed that the PFOA contained perflurocarboxylc acid (PFCA) impurities, including perfluorobutanoic acid (PFBA) (0.04 wt%), perfluoropentanoic acid (PFPeA) (0.17 wt%), perfluorohexanoic acid (PFHxA) (3.64 wt%), and perfluoroheptanoic acid (PFHpA) (13.8 wt%). Certified reference standards were used for quantitation of 1,4-dioxane (purity ≥ 97%) and perfluoro carboxylic acids (PFCAs) and were purchased from Accustandard (New Haven, CT, USA) and Wellington Laboratories (Overland Park, KS, USA), respectively. 5,5-dimethyl-1-pyrroline N-Oxide (DMPO, 97.0 +%) was obtained from TCI Chemicals (Portland, OR, USA) and 2,2,6,6-tetramethylpiperidine (TEMP) was purchased from Millipore Sigma (Burlington, MA, USA). Ammonium acetate solution (5 M, LC-MS grade) was purchased from Sigma-Aldrich (St. Louis, MO, USA). Ultrapure water (UHPLC-M grade) and methanol (LC-MS grade) were purchased from Thermo Fisher Scientific (Waltham, MA, USA) and isotopically labeled PFAS internal standards (perfluoro-n-($^{13}C_4$) butanoic acid, perfluoro-n-($^{13}C_5$) pentanoic acid, perfluoro-n-(1,2,3,4,6 - $^{13}C_5$) hexanoic acid, perfluoro-n-(1,2,3,4-$^{13}C_4$) heptanoic acid, and perfluoro-n-($^{13}C_8$) octanoic acid) were obtained from Wellington Laboratories (Overland Park, KS, USA).

2.2. Room temperature reactivity studies

Batch reactor experiments were carried out in triplicate in 1 L amber high-density polyethylene (HDPE) bottles at room temperature (22 ± 3 °C) using previously described methods (Manz et al., 2018, 2021). Solutions containing 1, 10, 15 and 20 g L^{-1} PAC were prepared in ultrapure water. The PAC was not washed prior to performing the experiments, thus; we did not remove any metal impurities. Solutions for the batch experiments contained the following: (1) ultrapure water (in all cases), (2) PFOA, PFHpA, PFHxA, PFPeA, and PFBA, (3) 1,4-dioxane, or (4) PFOA and 1,4-dioxane. For experiments with 1,4-dioxane and PFOA, controls without PAC were used to monitor losses to volatilization. The batch reactors were equilibrated for 96 h by mixing on a shaker. For low temperature experiments (5 and 11 ± 1 °C), the batch reactors were moved to a shaker in either an ice bath or refrigerator. After 96 h of total mixing and temperature stabilization, the batch reactors were spiked with potassium persulfate to initiate the reaction so that the final persulfate concentration was 75 mM. Potassium persulfate stock solutions were prepared 30 min prior to addition to the reactors. Experiments were carried out for a duration of 6–12 h and 10 mL aliquots of the reaction mixture were collected at each time point. The samples were pipetted into a 15 mL centrifuge tube containing 500 μL methanol to immediately quench the reaction of the radical species with PFCAs and 1,4-dioxane. The aliquots were immediately subjected to persulfate concentration analysis (Liang et al., 2008) (10 μL aliquots were added to 5 mL potassium iodide, described in the SI) and pH measurement. The pH was measured using a Mettler Toledo™ S220 SevenCompact™ pH/ion bench-top meter (Columbus, OH, USA). Sulfate (SO_4^{2-}) concentration was measured using a Metrohm 920 Absorber Module and 930 Compact IC Flex ion chromatograph (measurement details in the SI). Samples were filtered with a 0.2 μm syringe filter (Corning, Part No. 431224, Corning, NY, USA) and then diluted by taking 10 μL aliquots and adding 10 mL DI water. For measurement of the fluoride ion concentration, 1 mL aliquots were diluted in 1 mL of TISAB buffer and the concentration was measured using a fluoride selective probe (LOD = 0.5 μM) (Martínez-Mier et al., 2011; Tusl, 1972). The tubes were stored in a refrigerator at 4 °C and the mixture was centrifuged at 5000 rpm for 10 min prior to analysis. For the 1, 4-dioxane measurements, 3–5 mL of the supernatant was added to a GC-headspace vial containing 400 μL of methanol and 2 g of sodium chloride. For the measurement of PFCAs, 1 mL of the supernatant was pipetted into a 2 mL centrifuge tube containing 100 μL isotopically-labeled PFOA, PFHxA, PFHpA, PFPeA, and PFBA standards in methanol and extracted using a previously described liquid-liquid extraction procedure with methyl tert-butyl ether (Liu et al., 2020b). Details of the targeted analysis are described in the Supporting Information and Table S1. Non-targeted LC-MS analysis was performed to detect additional reaction byproducts and the methods used are described in the Supporting Information. Standard error of the data is represented in the figures using error bars, which was calculated by dividing the standard deviation by the square root of the number of observations. Details of the measurements used to determine persulfate, 1,4-dioxane, and PFCA concentrations are described in the Supporting Information. After reacting 15 g of PAC with 75 mM potassium persulfate for 24 h, the spent PAC was recovered using vacuum filtration with Grade 42 Whatman filter paper on a Buchner funnel. The spent PAC and fresh PAC were characterized and compared using FTIR to investigate oxygen-derived functional groups, XPS to characterize the surface chemistry, N_2 vapor isotherms to determine surface area and pore size distribution (PSD), and TGA to was used to quantify the mass loss when the samples are heated (see Supporting Information). Room temperature X-band (9.8 GHz) EPR spectroscopy measurements were performed on an EMX-plus *continuous-wave* (CW) spectrometer (Bruker BioSpin Corporation). DMPO and TEMP were used as the spin-trapping agent to probe the radical species in the reaction mixture containing persulfate and PAC. Details of the EPR methods used and spectral simulations are described in the Supporting Information.

2.3. PFAS Mass Balance

A mass balance experiment was performed at room temperature (22 ± 3 °C) to assess complete PFAS destruction. Solutions for the mass balance experiment contained the following: (1) ultrapure water (in all cases) and PFOA, (2) PFOA and 20 g L PAC^{-1}, and (3) PFOA, 20 g L PAC^{-1}, and 75 mM persulfate. The batch reactors were equilibrated for 96 h by mixing on a shaker prior to spiking with persulfate. The reaction was carried out for 24 h. Persulfate was measured at the end of the 24 h and was not detected. For each reactor, the aqueous phase was sampled and analyzed for PFCA concentration and inorganic fluoride concentration (analysis details in the SI). The PAC was recovered from the batch reactors were collected by vacuum filtration with Whatman filter paper (retains 2.7 μm particles and larger) on a Buchner funnel. PFCAs were extracted from 6 g of PAC using methyl tert-butyl ether (MTBE) as

previously reported (Al Amin et al., 2020; Zhang et al., 2021b). The extraction was performed by spiking the samples with internal standard, adding 5 mL MTBE, centrifuging for 5 min at 14,100g to remove particulates, transferring the supernatant to a new vial, and repeating for a total volume of 15 mL MTBE. The final extract was analyzed by LC-MS/MS (details in SI).

2. Results and discussion

2.1. Mechanism of persulfate activation by PAC

2.1.1. Persulfate activation batch studies

Persulfate activation at room temperature in ultrapure water at doses of 1, 10, 15, and 20 g L^{-1} PAC are shown in Fig. 1**a**. Although the initial concentration of persulfate was the same in all samples (75 mM), the experimental results indicated that the persulfate concentration decreased exponentially at higher PAC doses. The exponential decrease of the persulfate concentration suggested pseudo-first order kinetics in persulfate disappearance, which enabled the use of Eq. 5:

$$ln\left(\frac{C}{C_0}\right) = k_{obs} * t \quad (5)$$

where C is the persulfate concentration at a specific time, t, C_o is the initial persulfate concentration, and k_{obs} is the pseudo-first order reaction rate constant. The value of k_{obs} was determined by plotting the ln of the ratio C to C_o as a function of time (Fig. 1**b**) and the rate constants are presented in Table 1. With the exception of the plot with a 1 g L^{-1} dose of PAC ($R^2 = 0.81$), all of the plots were linear with R^2 values greater than 0.98. The reaction rate constants are plotted as a function of the PAC dose in Fig. 1**e**. The reaction rate increased exponentially with the PAC dose applied, and the pseudo-first order reaction rate constant, k_{obs}, was subsequently used to calculate the half-life of persulfate. The persulfate half-life decreased as the PAC dose increased, ranging from 0.92 to 63.8 h (Table 1). The pH profiles for these experiments are displayed in Fig. S1. As expected, pH rapidly decreased and remained around pH 1.1 throughout all of the conditions tested. Fig. S2 displays the production of sulfate (SO_4^{2-}) production during experiments with 20 g L^{-1} PAC and 75 mM potassium persulfate at 22 °C. After 4 h, the sulfate concentration appears to reach a maximum concentration, which coincides with persulfate depletion in Fig. 1**b**. The theoretical maximum sulfate concentration that could be produced by 75 mM persulfate is 150 mM (2 sulfate anions generate for every 1 persulfate anion). The maximum sulfate concentration detected was 135 mM, which is within 10 % experimental error, indicating that a ratio of persulfate added to sulfate generated was nearly 2:1.

Table 1
Pseudo-first-order reaction rate constants for persulfate activation as PAC dose increased.

Potassium Persulfate (mM)	PAC (g L^{-1})	T (°C)	k_{obs} (s^{-1})	$t_{1/2}$ (h)	R^2
75	1	22	3.06×10^{-6}	63.8	0.81
75	10	22	4.00×10^{-5}	4.82	0.99
75	15	22	1.19×10^{-4}	1.61	0.98
75	20	22	2.10×10^{-4}	0.92	1.00
75	20	5	6.70×10^{-5}	2.87	0.98
75	20	11	1.36×10^{-4}	1.42	0.99

Batch studies of persulfate activation were also performed at lower temperatures (5 and 11 °C) with 20 g L^{-1} PAC. The decay of persulfate at these temperatures and the natural log of the ratio C to C_o as a function of time are shown in Figs. 1**c** and 1**d**, respectively. As expected, higher temperatures led to higher rates of persulfate activation. However, persulfate activation was achieved at both 5 and 11 °C. This indicates that persulfate activation could be achieved using PAC in-situ in locations or during seasons where temperatures might be colder. Activation energy was calculated by creating an Arrhenius plot (Fig. S3), which relates the natural log of the reaction rate constants to the inverse of temperature (°K) and Eq. 6, where ΔG is the change in free energy and R is the ideal gas constant (J mol^{-1} K^{-1}). The calculated change in free energy was − 50.3 kJ mol^{-1}, indicating an exergonic reaction. However,

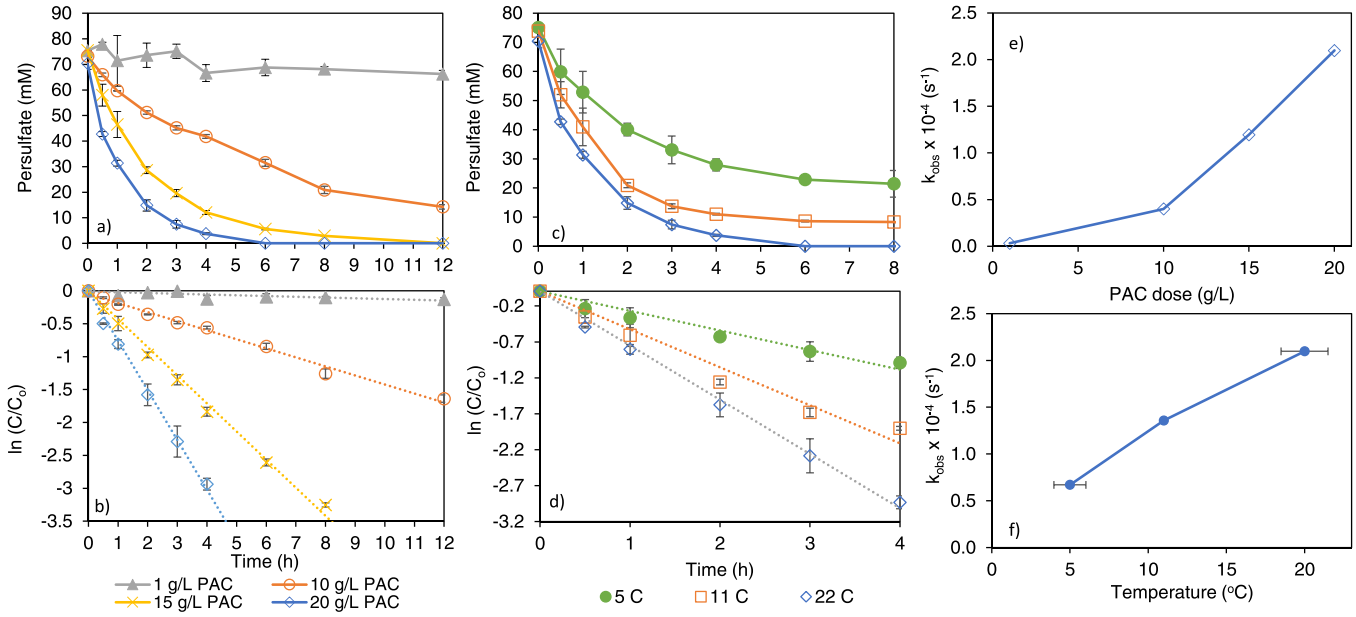

Fig. 1. (a) Decrease in persulfate concentration at room temperature (22 °C) with doses PAC ranging from 1 to 20 g L^{-1}. The initial persulfate concentration was 75 mM. The data was fitted to pseudo-first order kinetics, which are shown in (b). (c) Batch studies with 20 g L^{-1} PAC and 75 mM persulfate were repeated at 5 and 11 °C, with the pseudo-first order kinetics fits shown in (d). The trends of the observed reaction rate constants with the PAC dose and with temperature are displayed in (e) and (f), respectively. The error bars represent standard error (n = 3).

it is important to note that the temperature range was relatively small (10–25 °C) and the activation energy is likely to be PAC-dose dependent.

$$ln(k_{obs}) = -\frac{\Delta G^{\circ}}{RT} \quad (6)$$

2.1.2. PAC characterization

Spent PAC from the batch studies was recovered after persulfate was completely consumed and characterized relative to the fresh PAC sample. Shown in Fig. S4 are the results of TGA analysis on fresh PAC and spent PAC samples (PAC recovered after reacting 15 g L^{-1} PAC in the presence of 75 mM potassium persulfate for 12 h at room temperature) that were heated to 950 °C in an inert gas and cooled to room temperature. The spent PAC sample displayed large mass losses as the temperature was increased from 220 °C and 600 °C in comparison to the fresh PAC sample, which did not undergo any loss of mass. Persulfate and oxygen-derived functional groups were removed in the form of SO_2 and CO/CO_2 upon heating the spent PAC sample.

The N_2 adsorption isotherms (Fig. S5) at 77 K were used to calculate specific surface areas using the BET equation. As expected, the specific surface area of fresh PAC was as high as 915 m^2 g^{-1} in comparison to the spent PAC, which had a specific surface area of 398 m^2 g^{-1}. This indicates a substantial reduction (58 %) in the available surface area of spent PAC. The pore size distribution (PSD) of both samples is shown in Fig. S6, where the PSD confirms the surface area loss in the spent PAC. The pore space that was lost was primarily microporosity (< 2 nm). Moreover, the micropore volume calculated from N_2 isotherm data using the Dubinin-Radushkevich (DR) equation decreased from 0.342 cc g^{-1} in fresh PAC to 0.149 cc g^{-1} in spent PAC. The reduction in micropore volume was consistent with the 58 % loss of surface area of spent PAC. Heating of the spent PAC to 950 °C showed partial of the surface area and porosity, The oxygen-derived functional groups and persulfate moieties that were released from the PAC surface during persulfate activation may have resulted in the release of gaseous carbon, which altered the microporosity of the parent sample.

FTIR spectra (Fig. S7) displayed peaks at 1160 cm^{-1} and 1715 cm^{-1} in spent PAC that were indicative of the presence of the oxygen-derived functional groups, epoxide (C-O) and carboxyl or ketones (C═O), respectively. The adjacent peak observed in fresh PAC at 1585 cm^{-1} is commonly attributed to the vibration frequency of a pristine graphenic domain (C═C). As expected, the fresh PAC FTIR spectrum only displayed the C═C vibrations at 1585 cm^{-1}, suggesting the absence of significant oxygen-derived functionalities. Shown in Fig. S8 and Table S2 are the results of the XPS analysis of the spent PAC and PAC samples. The spent PAC sample showed weak potassium binding energies (Fig. S8) and ~ 2.9 atom % of sulfur, indicating the presence of potassium and persulfate. The XPS results also revealed a high level of oxidation for spent PAC with a C:O ratio of 4.3:1, in comparison with a C:O ratio of 18.1:1 for the fresh PAC. These findings present unambiguous evidence that there was severe oxidation of the PAC surface during persulfate activation. Furthermore, these bonds were broken when heated to 950 °C by an inert gas. Thus, **Reactions 4** and **5** in **Scheme 1** could not be the primary mechanism for organic contaminant degradation using PAC and persulfate because of the absence of oxygen-derived functional groups on the PAC surface.

2.1.3. Mechanism of persulfate activation by PAC

EPR spectroscopy was used to explore radical formation during room temperature persulfate activation by PAC. Fig. 2**a** displays the experimental EPR spectra of a mixture of 75 mM potassium persulfate with 140 mM DMPO, 15 g L^{-1} PAC with 140 mM DMPO, and 15 g L^{-1} PAC and 75 mM potassium persulfate with 140 mM DMPO. Previous EPR studies had suggested that the activation of persulfate by PAC is non-radical forming (Yao et al., 2019) due to the absence of EPR signals with the spin trapping agent, DMPO, at ambient temperature. However, it is possible that the concentrations of persulfate (2.5 mM) and DMPO (100 nM) employed were too low, and the radical adducts were absorbed or quenched by AC. Thus, a higher persulfate concentration was used in the present study in conjunction with two control experiments (Fig. 2). The first control in the presence of PAC and DMPO did not result in EPR signals, suggesting no spins were captured. The second control with persulfate and DMPO generated EPR signals. As shown in Fig. 2, the resulting EPR spectrum indicated the formation of DMPO-SO_4 (six lines, 1:1:1:1:1:1) and DMPO-OH (four lines 1:2:2:1). Although the peak intensity was low, these data indicate the generation of $SO_4^{\cdot-}$ and $OH^{\cdot}$ without the addition of PAC. A mixture of PAC and DMPO in the

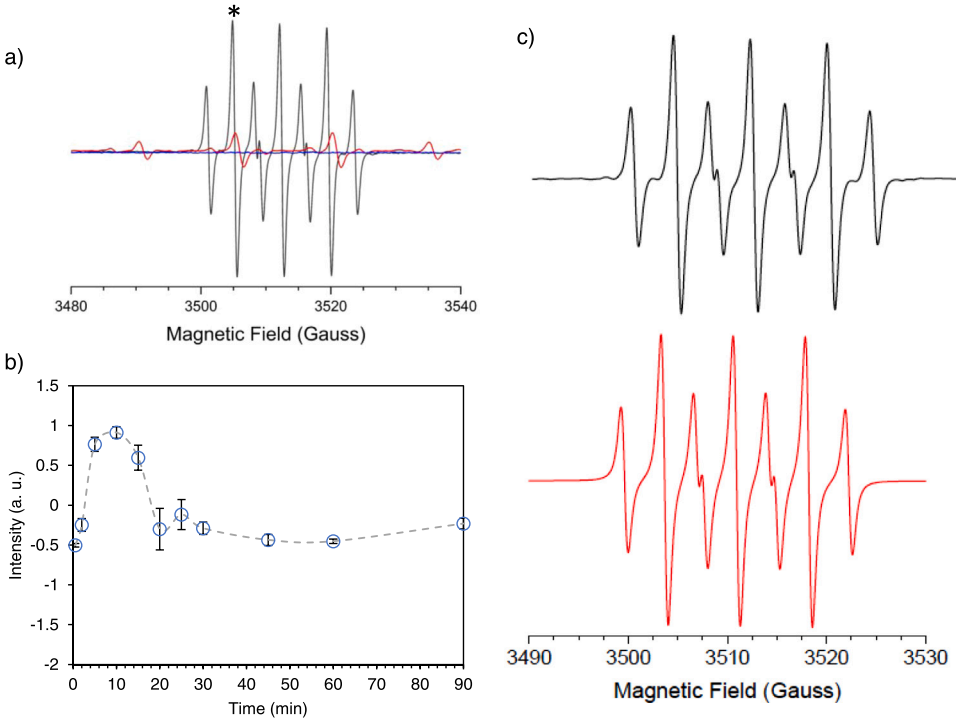

Fig. 2. EPR spectrum of radical adduct formed with 140 mM spin trapping agent DMPO in 20 °C batch studies with both 15 g L^{-1} PAC and 75 mM persulfate (black line), 75 mM persulfate and no PAC (red line), and 15 g L^{-1} PAC and no persulfate (blue line) shown in (a) after 30 min of reacting. The formation of the radical adduct over time is displayed in (b). The intensity plotted is the peak intensity of the peak labeled with a * in (a). Experimental (top) and simulated (bottom) EPR spectrum of a mixture of 15 g L^{-1} PAC and 140 mM DMPO with 75 mM potassium persulfate are displayed in (c). The spectral simulation using a single component fit yielded ^{14}N and ^{1}H hyperfine coupling constants of 7.27 G and 4.04 G, respectively.

presence of persulfate resulted in stronger EPR signals (Fig. 2), however, the line shape pattern was not characteristic of hydroxyl or sulfate (DMPO-OH or DMPO-SO_4) (Fagan et al., 2022). We performed numerical simulations to determine the identity of the radical species that resulted in the strong EPR signals in Fig. 2**a**. As can be seen in Fig. 2**c**, the simulated spectral line shape is in excellent agreement with the experimental spectrum obtained from the mixture of PAC and DMPO in the presence of persulfate. The ^{14}N and ^{1}H hyperfine coupling constants, A_N and A_{H1}/A_{H2} for the nitrogen and gamma hydrogen atoms of DMPO, were 7.27 G and 4.04 G, respectively. The ^{14}N hyperfine coupling constant of 7.27 G has been shown to be characteristic of a DMPOX radical species (Barr and Mason, 1995; Buettner, 1987). Thus, the spectral simulations confirmed that the radical adduct formed in PAC activation of persulfate was 5,5-dimethylpyrrolidone-2(2)-oxyl-(1) (DMPOX). Previous studies have indicated that DMPOX is an oxidized derivative of DMPO (Xiao et al., 2021). DMPOX has been observed when carbon nanotubes, copper oxide, and metal nanoparticles were used to activate persulfate (Ahn et al., 2016; Lee et al., 2015; Li et al., 2019). The formation of DMPOX does not necessarily indicate that hydroxyl and sulfate radicals are absent; rather, it is an indication that DMPO, DMPO-OH, or DMPO-SO_4 is oxidized much more rapidly than the formation of the primary radical adducts (Bilski et al., 1996; Huang and Zhang, 2019; Xie et al., 2019). Spin trap experiments were also performed with TEMP to probe singlet oxygen as the nonradical species that could lead to the formation of DMPOX. Fig. S9 displays the experimental EPR spectra of a mixture of 75 mM potassium persulfate with 100 mM TEMP, 15 g L^{-1} PAC with 100 mM TEMP, and 15 g L^{-1} PAC and 75 mM potassium persulfate with 100 mM TEMP. TEMP is a spin trapping agent that reacts preferentially with singlet oxygen to form a stable nitroxide radical, 2,2,6,6-tetramethylpiperineN-oxyl (TEMPO). A strong EPR signal (three lines 1:1:1) was observed in all conditions, including the controls. These results indicate that the DMPOX EPR signal is not related to singlet oxygen generation, as the TEMPO triplet was observed even in control experiments.

We replicated the spin trapping experiments with persulfate and PAC to study the formation of DMPOX over time. As the reaction of persulfate and PAC continued, EPR spectra of aliquots of the reaction mixture were measured at regular time intervals (Fig. 2**b** and **S10**). The spectra obtained after the initial mixing indicate that there was no change in the radical species after 30 s, which suggests that DMPOX was formed in less than 30 s. The intensity of the EPR signals increased for the first 10 min, followed by a decrease in intensity, and sustained intensity from 20 to 90 min. Taken in concert, these results suggest the activation of persulfate and formation of ROS was sustained.

Previous studies have reported that DMPO-SO_4 is highly unstable and immediately transforms to DMPOX (Du et al., 2019; Maeno et al., 2015). Thus, rapid production of sulfate radicals likely leads to the presence of a strong DMPOX EPR signal that was only observed when both PAC and persulfate were present. $SO_4^{\cdot-}$ has strong reactivity with unsaturated bonds and shows a stronger tendency for electron extraction than $OH^{\cdot}$ (Huang et al., 2021). Hydroxyl radicals are unlikely to be present, as the PAC/PS system efficiently degraded PFOA (data presented in the next section) and the hydroxyl radical is not reactive with PFAS (Hori et al., 2008; Javed et al., 2020; Liao and Farrell, 2009; Patch et al., 2022; Szajdzinska-Pietek and Gebicki, 2000; Vecitis et al., 2009). However, the sulfate radical effectively degrades PFCAs (Lutze et al., 2018; Sühnholz et al., 2021; Yang et al., 2020). Prior to the oxidation reaction, the PAC consisted of pristine graphene, which has C═C. After the reaction, the composition of the PAC changed, and an increase C-O was observed. C═C has π bonds localized above and below the C-C σ bond. The π bonds are loosely bound, which allows an electrophile to attract the electrons and form a new bond. Thus, PAC serves as an electron donor in an oxidation-reduction reaction with persulfate (**Reaction 5**). As the C═C bonds in the PAC are oxidized, persulfate accepts the electrons from the π bonds, and the reduction reaction results in the formation of a sulfate radical. As evidenced by the production of sulfate (Fig. S2), the peroxide bond in persulfate is cleaved. Thus, we propose that the primary mechanism of persulfate activation is an oxidation-reduction reaction where direct electron transfer from the PAC results in reduction of persulfate to form a sulfate radical (**Reaction 7**).

$$PACsurface - C = C \quad + \quad S_2O_8^{2-} \rightarrow \quad SO_4^{\cdot-} + \quad SO_4^{2-} \\ + \quad PACsurface - C - C - OH \tag{7}$$

2.2. Application of the PAC/persulfate system to degrade PFOA and 1,4-dioxane

2.2.1. Removal of 1,4-dioxane and PFOA at temperatures less than 25 °C

Prior to performing experiments with PAC, a control batch study (no persulfate, no PAC) was performed with 1,4-dioxane, PFOA, and persulfate. No persulfate activator was used, and the temperature was maintained at 20 °C for 240 h. The initial pH of 7 was not adjusted at the start of the experiment. The PFOA, dioxane, and persulfate concentrations are displayed in Fig. 3**.** As expected, without an activator, the persulfate concentration did not decrease, indicating that no persulfate activation occurred. 1,4-dioxane was easily oxidized by persulfate, an expected result based on prior studies (Félix-Navarro et al., 2007). Despite reports that demonstrate PFOA can be degraded by persulfate in solutions with an initial pH between 2.5 and 7.1 (Lee et al., 2012a), PFOA did not degrade in our experiment. We surmise that persulfate was not activated at this temperature without an activator; thus, an insufficient amount of $SO_4^{\cdot-}$ was produced to degrade PFOA. However, it is plausible that the 1,4-dioxane competed in the reaction and reacted preferentially with any $SO_4^{\cdot-}$ that formed.

Batch studies were performed with PAC, persulfate, and PFOA and/or 1,4-dioxane at room temperature to evaluate the effectiveness of the combining PAC and persulfate to destroy contaminants at low temperatures. Prior to experiments with the addition of persulfate, adsorption equilibrium experiments were performed for both PFOA and 1,4-dioxane over 96 h (Fig. S11) to determine the length of time required for adsorption to occur. Control experiments were also performed to

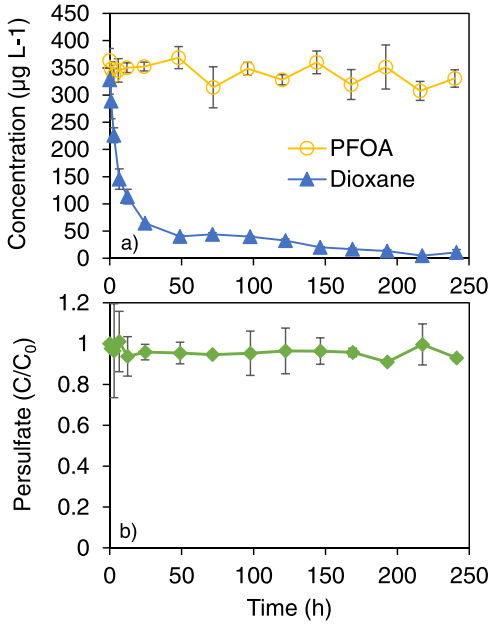

Fig. 3. Competitive reaction of 1,4-dioxane and PFOA at room temperature (20 °C) with 75 mM persulfate over 240 h (no activator used in this experiment). Persulfate did not decompose over the 240 h, indicating no activation occurred. 1,4-dioxane decreased, and the samples taken after 200 h are <LOD. No decrease in PFOA concentration was observed. Error bars represent standard error (n = 3).

monitor for volatile losses. 1,4-dioxane reached adsorption equilibrium within 24 h of mixing, while PFOA adsorption equilibrium was reached within 96 h. Therefore, prior to adding persulfate to initiate the oxidation reaction, PFOA and/or 1,4-dioxane were mixed with the PAC for a minimum of 96 h to allow sorption of PFAS to occur prior to persulfate addition. In these experiments, a greater amount of PFOA was adsorbed to the PAC than 1,4-dioxane. The PFOA concentration decreased from 3500 μ L^{-1} to 0.2 μ L^{-1}, while 1,4-dioxane decreased from 1400 μ L^{-1} to 445 μ L^{-1}. This observation was expected and is consistent with the log K_{ow} values (−0.271 for 1,4-dioxane and 3.10 for PFOA). PFOA has a higher log K_{ow} value than 1,4-dioxane, indicating PFOA is more hydrophobic than 1,4-dioxane and has a higher tendency to adsorb to PAC."

Experiments with both PFOA and 1,4-dioxane present as co-contaminants in the initial solution were carried out at 11 °C and room temperature (22 °C) using PAC as an activator. Adsorption equilibrium was established with PAC for 96 h at room temperature in triplicate prior to spiking the reactors with persulfate. Following adsorption, the concentration of PFOA was 40 nM and 1,4-dioxane concentration was 450 nM. Short chain PFCAs were detected in the initial solutions in low concentrations due to impurities in the PFOA (PFBA, PFPeA, and PFHxA ≤ LOD, and PFHpA = 0.035 nM). Following adsorption at 11 °C, the initial concentrations were 2240 nM PFOA and 1.38 nM PFHxA (PFBA, PFPeA, and PFHpA < LOD). After 96 h of mixing, the solutions were spiked with persulfate (75 mM, room temperature). The 11 °C experiment was carried out for 8 h while the room temperature experiment was carried out for 6 h. There was a decrease in the PFOA and 1,4-dioxane concentrations at both 11 °C and room temperature (Fig. 4). As PFOA degraded, shorter chain length carboxylic acids were formed at both reaction temperatures, as indicated by an increase in their concentrations. Initially PFHpA appeared in the room temperature experiment, followed by the formation of PFHxA, PFPeA, and finally PFBA. The same pattern was observed at 11 °C; however, PFBA was < LOD throughout the experiment. The fluoride ion concentrations were less than the limit of detection throughout the entire experiment.

2.2.2. PFAS mass balance

To assess PFAS destruction, additional batch experiments were carried out at room temperature (22 °C) and sampled after 24 h. Two control experiments were completed alongside the reactors containing PFOA, 20 g L^{-1} PAC, and 75 mM persulfate. In the PFOA only control, PFBA, PFPeA, PFHxA, PFHpA, and PFOA were detected in the aqueous phase (no PAC was added). In the control containing PFOA and PAC, all 5 PFCAs (PFBA, PFPeA, PFHxA, PFHpA, and PFOA) were detected in both the aqueous phase and PAC extract. In the experiment containing PAC and persulfate, high concentrations (18.9 μmol L^{-1}) of fluoride were detected. All concentrations detected were converted to fluoride equivalents (in μmol) and are displayed in Table S3 and Fig. S12. In the PAC control, 84 % of the total amount of fluorine was recovered, and in the PAC and persulfate experiment 86 % was recovered.

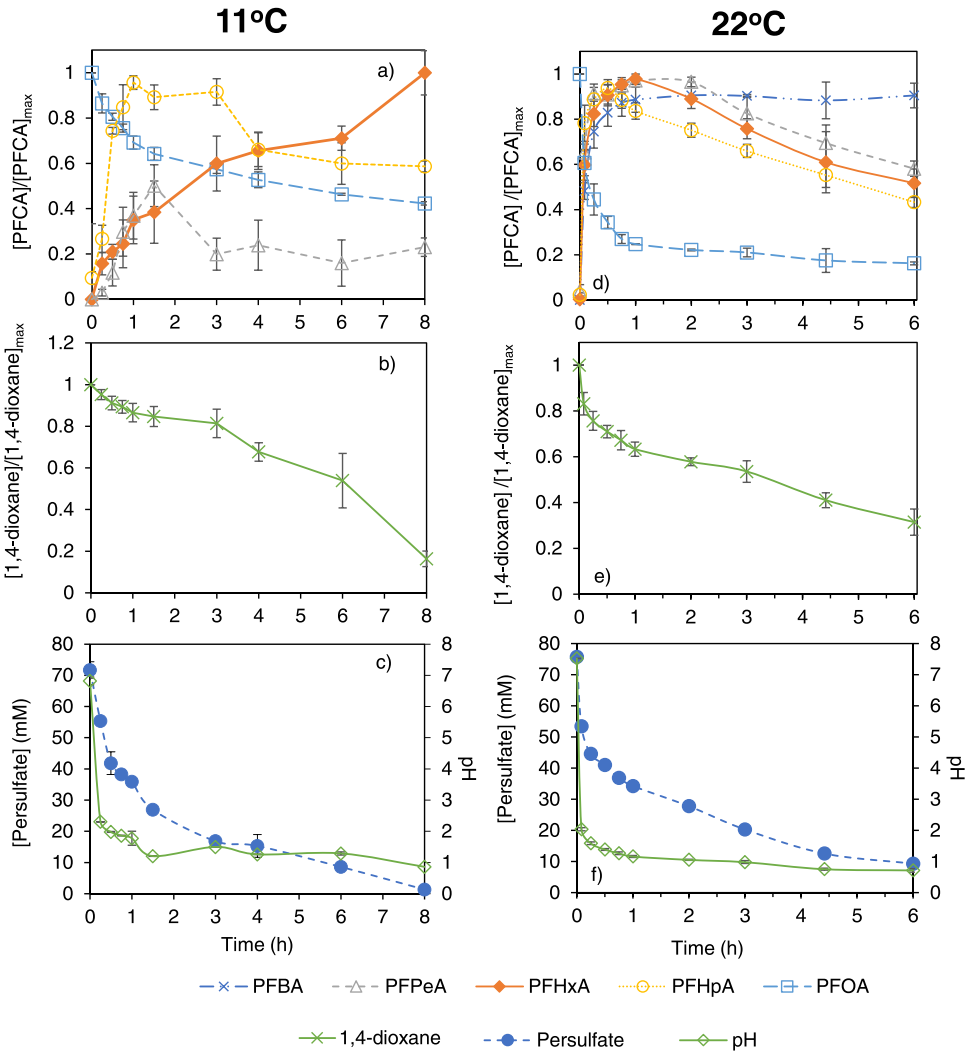

Fig. 4. Competitive reaction of 1,4-dioxane and PFOA in 20 g L^{-1} PAC and 75 mM persulfate at 11 °C and room temperature over 8 and 6 h, respectively. PFOA degraded into shorter chain PFCAs as displayed in (a) and (d). In the 11 °C experiment, after adsorption for 96 h, the initial PFOA concentration was 2240 nM. PFBA, PFPeA, PFHxA, and PFHpA impurities found in the 11 °C solution after adsorption were quantified and were <LOD, <LOD, 1.38, <LOD nM, respectively. Where concentrations are represented by C/C_{max}, the maximums for the 11 °C experiment were: 1.57 mM PFHpA, 15.1 nM PFHxA, and 191 nM PFPeA. In room temperature experiments, after adsorption for 96 h, the initial PFOA concentration was 40 nM. PFBA, PFPeA, PFHxA, and PFHpA impurities found in the solution after adsorption were quantified and were < LOD, < LOD, < LOD, 0.035 nM, respectively. Where concentrations are represented by C/C_{max}, the maximums for the 22 °C experiment were: 1.20 mM PFHpA, 10.7 nM PFHxA, 0.376 nM PFPeA, and 0.148 nM PFBA. As this experiment was performed with a lower initial PFOA concentration, fluoride remained < LOD throughout both experiments. The presence of PFCAs slowed down 1,4-dioxane degradation (initial concentration after PAC adsorption was 450 nM). Error bars represent standard error (n = 3).

2.2.3. PFOA degradation pathway discussion

The batch studies discussed above were repeated with PFOA alone at a higher concentration to gain a better understanding of the mechanism of PFOA degradation (initial concentrations were 6.84 $\times 10^{-2}$ μM PFBA, 2.60 $\times 10^{-1}$ μM PFPeA, 3.46 μM PFHxA, 12.8 μM PFHpA, and 67.1 μM PFOA). The concentrations after adsorption, prior to spiking with persulfate, were 8.80 $\times$ 10^{-3} μM PFBA, 2.6 $\times$ 10^{-2} μM PFPeA, 2.19 μM PFHxA, 0.128 μM PFHpA, and 25.9 μM PFOA. The persulfate concentration and pH profiles are shown in Fig. S13. The persulfate concentration and pH decreased over 6 h in the persulfate batch studies. Fig. S14a shows the change in PFOA, PFHxA, PFHpA, PFPeA, and PFBA concentration after persulfate was added at room temperature. PFOA decomposed rapidly (1970 nM initial concentration after adsorption) with 97 % removal within 6 h of the initial reaction. Similarly, the concentration of PFHxA and PFHpA also decreased by 72% and 76%, respectively (the initial concentrations after adsorption were 17 nM PFHpA and 219 nM PFHxA). The concentration of the shorter chain length PFCAs, PFBA and PFPeA (2.05 nM and 219 nM, respectively, initial concentration after adsorption) increased over the course of the 6 h reaction, as did the concentration of fluoride ions (Fig. S14b). Prior to adding persulfate, the total molar concentration of fluorine in solution attributed to PFOA, PFHpA, PFHxA, PFPeA, and PFBA was 32,140 nM. Fluoride ions were not detected in the initial samples and reached 5320 nM maximum concentration (17 % of the potential maximum). Thus, complete PFCA mineralization did not occur. Using non-targeted LC-HRMS analysis, additional byproducts were detected (Table S4), including perfluoroheptanal (Fig. S15). Perfluoroheptanal peak area reached a maximum at 30 min. Additional byproducts may have formed that were not detected by LC-HRMS due to volatility, adsorption to the PAC, or low stability.

Combining the targeted PFCA data and non-targeted analysis, we propose PFOA degradation pathway (Fig. 5) in the persulfate/PAC system. First, PFOA adsorbs to the PAC. When persulfate is added, the persulfate is activated by the PAC to form a sulfate radical (**Reaction 5**), which initiates the unzipping of PFOA (loss of a CF_2 unit). The unzipping reaction was revealed by detection of the generated PFCAs (PFHpA, PFHxA, PFPeA, and PFBA). Detection of perfluoroheptanal gave insight into the intermediates that may form in the unzipping reaction. Decarboxylation of PFOA is initiated by sulfate radical attack, which transfer an electron to PFOA to form a perfluoroalkyl radical. The perfluoroalkyl radical continues to react to form the perfluoro alcohol, which is unstable and undergoes HF elimination to form perfluoroheptanal. Perfluoroheptanal is then oxidized to form PFHpA, and this mechanism is repeated until PFOA is eventually converted to PFBA. PFBA could be further transformed to form F- and CO_2.

3. Conclusions

The results of this work provide direct evidence that PAC activates persulfate at ambient temperatures, resulting in degradation of PFOA and 1,4-dioxane, which commonly occur in groundwater as co-contaminants. In contrast to traditional methods used for persulfate activation (e.g., heat, ultra-violet light, and electrolysis), activation using PAC does not rely on an external energy source. Thus, a treatment combining AC and persulfate has the potential to remediate contaminants in-situ in the absence of an activation agent or subsurface heating, both of which can be prohibitively expensive. The observed activation of persulfate using PAC also occurred at lower temperatures (5 or 11 °C), confirming relevance to natural groundwaters. EPR spectroscopy demonstrated that DMPO was rapidly oxidized to DMPOX, indicating that highly oxidative radical species, likely sulfate radicals, were formed during persulfate activation using PAC at room temperature. EPR studies with TEMP demonstrated that singlet oxygen is not the primary reactive oxygen species that leads to the formation of DMPOX. Taken in concert, the EPR, PAC characterization, and activation data indicate sulfate radical formation which resulted in rapid PFOA and 1,4-dioxane

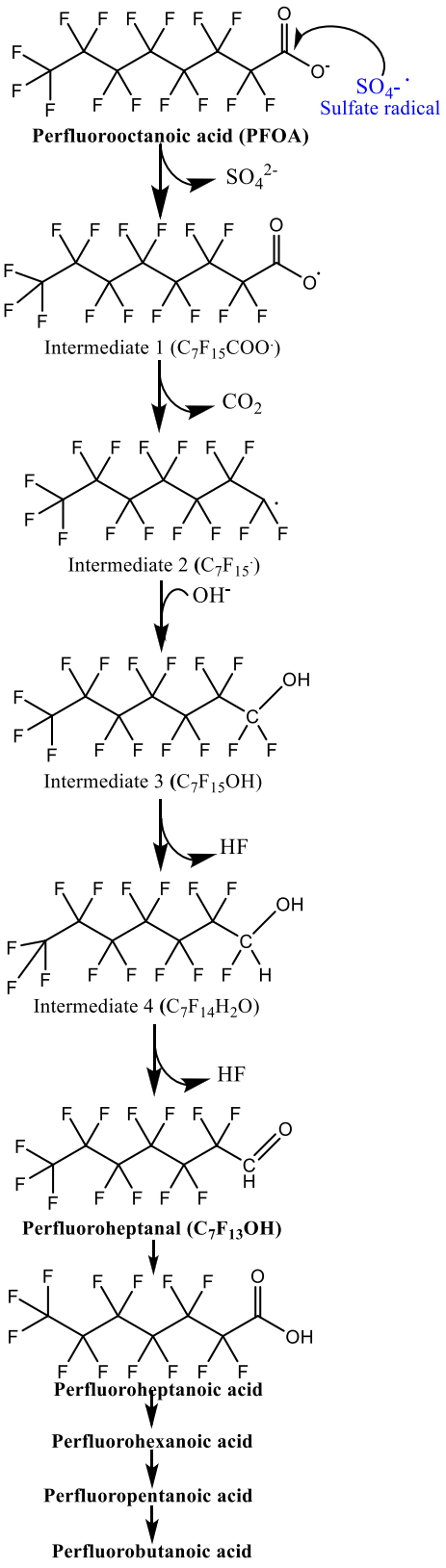

Fig. 5. Proposed mechanism for PFOA transformation in the persulfate/PAC system at room temperature. PFOA and shorter chain carboxylic acids were detected in targeted analysis, while perfluoroheptanal, was detected by non-targeted analysis. PFOA is transformed to form PFHpA and the reaction steps are repeated until PFBA forms.

degradation. In potential field applications, persulfate and PAC could be delivered in-situ to create a PRB that is able to simultaneously sequester and destroy contaminants. Previous studies have demonstrated that PAC is readily injectable into the subsurface and retained in quartz sands and soils (Liu et al., 2020a). Therefore, treatment by persulfate and PAC could be implemented by creating a PAC zone in the subsurface and then injecting or mixing persulfate immediately up gradient from the PAC zone. Additional studies with aquifer solids and natural soils are underway to further evaluate the potential applicability of the PAC/PS treatment for in-situ groundwater remediation.

Environmental Implications

We demonstrate the activation of persulfate using powder activated carbon (PAC) at temperatures relevant to ground water (5 – 22 °C). Electron paramagnetic resonance spectroscopy with spin trapping agents showed that singlet oxygen was the primary reactive oxygen species that leads to contaminant degradation. The method is applied to simultaneously degrade perfluorooctanoic acid and 1,4-dioxane at low temperatures. In contrast to the common persulfate activation methods, activation using PAC does not rely on an external energy source. Thus, a treatment combining AC and persulfate can potentially remediate contaminants in-situ in the absence of external energy at the subsurface, which can be prohibitively expensive.

CRediT authorship contribution statement

K. E. Manz: Conceptualization, Methodology, Validation, Formal Analysis, Investigation, Resources, Writing - Original Draft, Writing - Review & Editing, Visualization; **I. Kulatos:** Formal Analysis, Investigation, Writing - Original Draft, Writing - Review & Editing, Visualization; **C. A. Greenley:** Investigation, Resources, Writing - Review & Editing, Visualization; **P. J. Landry:** Formal Analysis, Investigation, Visualization; **K. V. Lakshmi**: Formal Analysis, Investigation, Writing - Review & Editing; **M. Woodcock:** Formal Analysis, Investigation; **L. Hellerich:** Conceptualization, Methodology, Resources, Writing - Review & Editing; **J. D. Bryant:** Conceptualization, Methodology, Resources, Writing - Review & Editing; **M. Apfelbaum:** Conceptualization, Resources, Writing - Review & Editing; **K. D. Pennell:** Conceptualization, Methodology, Resources, Writing - Original Draft, Writing - Review & Editing.

Declaration of Competing Interest

The authors declare that they have no known competing financial interests or personal relationships that could have appeared to influence the work reported in this paper.

Data availability

Data will be made available on request.

Acknowledgments

The authors would like to thank the Instrumentation for Molecular and Nanoscale Innovation (IMNI) at Brown University NanoTools Facility (NTF) and Dr. Hector Garces for training and use of the EPR instrument. This work was supported by funding from Woodard & Curran and the NIEHS Training in Environmental Pathology T32 program (grant #T32 ES007272). The high-resolution mass spectrometer used to identify reaction byproducts was partially funded by NSF Major Research Instrumentation (MRI) award CBET-1919870.

Appendix A. Supporting information

Supplementary data associated with this article can be found in the online version at doi:10.1016/j.jhazmat.2022.129966.

References

Abunada, Z., Alazaiza, M.Y.D., Bashir, M.J.K., 2020. An overview of per- and polyfluoroalkyl substances (pfas) in the environment: source, fate, risk and regulations. Water 12 (12), 3590.
Adamson, D.T., Piña, E.A., Cartwright, A.E., Rauch, S.R., Hunter Anderson, R., Mohr, T., Connor, J.A., 2017. 1,4-dioxane drinking water occurrence data from the third unregulated contaminant monitoring rule. Sci. Total Environ. 596–597, 236–245.
Ahn, Y.-Y., Yun, E.-T., Seo, J.-W., Lee, C., Kim, S.H., Kim, J.-H., Lee, J., 2016. Activation of peroxymonosulfate by surface-loaded noble metal nanoparticles for oxidative degradation of organic compounds. Environ. Sci. Technol. 50 (18), 10187–10197.
Al Amin, M., Sobhani, Z., Liu, Y., Dharmaraja, R., Chadalavada, S., Naidu, R., Chalker, J. M., Fang, C., 2020. Recent advances in the analysis of per- and polyfluoroalkyl substances (pfas)—a review. Environ. Technol. Innov. 19, 100879.
Annamalai, S., Septian, A., Choi, J., Shin, W.S., 2022. Remediation of phenol contaminated soil using persulfate activated by ball-milled colloidal activated carbon. J. Environ. Manag. 310, 114709.
Barr, D.P., Mason, R.P., 1995. Mechanism of radical production from the reaction of cytochrome c with organic hydroperoxides.: an esr spin trapping investigation*. J. Biol. Chem. 270 (21), 12709–12716.
Bilski, P., Reszka, K., Bilska, M., Chignell, C.F., 1996. Oxidation of the spin trap 5,5-dimethyl-1-pyrroline n-oxide by singlet oxygen in aqueous solution. J. Am. Chem. Soc. 118 (6), 1330–1338.
Bruton, T.A., Sedlak, D.L., 2017. Treatment of aqueous film-forming foam by heat-activated persulfate under conditions representative of in situ chemical oxidation. Environ. Sci. Technol. 51 (23), 13878–13885.
Buettner, G.R., 1987. Spin trapping: Esr parameters of spin adducts 1474 1528v. Free Radic. Biol. Med. 3 (4), 259–303.
Cashman, M.A., Kirschenbaum, L., Holowachuk, J., Boving, T.B., 2019. Identification of hydroxyl and sulfate free radicals involved in the reaction of 1,4-dioxane with peroxone activated persulfate oxidant. J. Hazard. Mater. 380, 120875.
Coyle, C., Ghosh, R., Leeson, A., Thompson, T., 2021. Us department of defense–funded research on treatment of per- and polyfluoroalkyl substance–laden materials. Environ. Toxicol. Chem. 40 (1), 44–56.
Du, J., Bao, J., Liu, Y., Kim, S.H., Dionysiou, D.D., 2019. Facile preparation of porous mn/fe3o4 cubes as peroxymonosulfate activating catalyst for effective bisphenol a degradation. Chem. Eng. J. 376, 119193.
Duan, X., Ao, Z., Zhou, L., Sun, H., Wang, G., Wang, S., 2016. Occurrence of radical and nonradical pathways from carbocatalysts for aqueous and nonaqueous catalytic oxidation. Appl. Catal. B: Environ. 188, 98–105.
Duan, X., Sun, H., Wang, S., 2017. Comment on "activation of persulfate by graphitized nanodiamonds for removal of organic compounds". Environ. Sci. Technol. 51 (9), 5351–5352.
Evans, P.J., Dugan, P., Nguyen, D., Lamar, M., Crimi, M., 2019. Slow-release permanganate versus unactivated persulfate for long-term in situ chemical oxidation of 1,4-dioxane and chlorinated solvents. Chemosphere 221, 802–811.
Fagan, W.P., Villamena, F.A., Zweier, J.L., Weavers, L.K., 2022. In situ epr spin trapping and competition kinetics demonstrate temperature-dependent mechanisms of synergistic radical production by ultrasonically activated persulfate. Environ. Sci. Technol.
Fang, G., Liu, C., Gao, J., Dionysiou, D.D., Zhou, D., 2015. Manipulation of persistent free radicals in biochar to activate persulfate for contaminant degradation. Environ. Sci. Technol. 49 (9), 5645–5653.
Félix-Navarro, R.M., Lin-Ho, S.W., Barrera-Díaz, N., Pérez-Sicairos, S., 2007. Kinetics of the degradation of 1,4-dioxane using persulfate. Rev. De. la Soc. Quím. De. Mex. 51, 67–71.
Forouzesh, M., Ebadi, A., Aghaeinejad-Meybodi, A., 2019. Degradation of metronidazole antibiotic in aqueous medium using activated carbon as a persulfate activator. Sep. Purif. Technol. 210, 145–151.
Furman, O.S., Teel, A.L., Watts, R.J., 2010. Mechanism of base activation of persulfate. Environ. Sci. Technol. 44 (16), 6423–6428.
Hori, H., Nagaoka, Y., Murayama, M., Kutsuna, S., 2008. Efficient decomposition of perfluorocarboxylic acids and alternative fluorochemical surfactants in hot water. Environ. Sci. Technol. 42 (19), 7438–7443.
Huang, K.Z., Zhang, H., 2019. Direct electron-transfer-based peroxymonosulfate activation by iron-doped manganese oxide (δ-mno2) and the development of galvanic oxidation processes (gops). Environ. Sci. Technol. 53 (21), 12610–12620.
Huang, W., Xiao, S., Zhong, H., Yan, M., Yang, X., 2021. Activation of persulfates by carbonaceous materials: a review. Chem. Eng. J. 418, 129297.
Javed, H., Lyu, C., Sun, R., Zhang, D., Alvarez, P.J.J., 2020. Discerning the inefficacy of hydroxyl radicals during perfluorooctanoic acid degradation. Chemosphere 247, 125883.
Kambhu, A., Gren, M., Tang, W., Comfort, S., Harris, C.E., 2017. Remediating 1,4-dioxane-contaminated water with slow-release persulfate and zerovalent iron. Chemosphere 175, 170–177.
Kolthoff, I.M., Miller, I.K., 1951. The chemistry of persulfate. I. The kinetics and mechanism of the decomposition of the persulfate ion in aqueous medium1. J. Am. Chem. Soc. 73 (7), 3055–3059.
Lee, H., Lee, H.-J., Jeong, J., Lee, J., Park, N.-B., Lee, C., 2015. Activation of persulfates by carbon nanotubes: oxidation of organic compounds by nonradical mechanism. Chem. Eng. J. 266, 28–33.

Lee, Y., Lo, S., Kuo, J., Hsieh, C., 2012b. Decomposition of perfluorooctanoic acid by microwaveactivated persulfate: effects of temperature, ph, and chloride ions. Front. Environ. Sci. Eng. 6 (1), 17–25.
Lee, Y.C., Li, Y.F., Lo, S.L., Kuo, J., Sun, W., Hu, C.Y., 2022. Decomposition of perfluorooctanic acid by carbon aerogel with persulfate. Chem. Eng. J. 430, 132900.
Lee, Y.-C., Lo, S.-L., Kuo, J., Lin, Y.-L., 2012a. Persulfate oxidation of perfluorooctanoic acid under the temperatures of 20–40°C. Chem. Eng. J. 198–199, 27–32.
Lee, Y.-C., Lo, S.-L., Kuo, J., Huang, C.-P., 2013. Promoted degradation of perfluorooctanic acid by persulfate when adding activated carbon. J. Hazard. Mater. 261, 463–469.
Lee, Y.-C., Li, Y.-f, Chen, M.-J., Chen, Y.-C., Kuo, J., Lo, S.-L., 2020. Efficient decomposition of perfluorooctanic acid by persulfate with iron-modified activated carbon. Water Res. 174, 115618.
Li, M., Fiorenza, S., Chatham, J.R., Mahendra, S., Alvarez, P.J.J., 2010. 1,4-dioxane biodegradation at low temperatures in arctic groundwater samples. Water Res. 44 (9), 2894–2900.
Li, W., Wu, Y., Gao, Y., Xing, S., 2019. Mechanism of persulfate activation with cuo for removing cephalexin and ofloxacin in water. Res. Chem. Intermed. 45 (11), 5549–5558.
Liang, C., Huang, C.-F., Mohanty, N., Kurakalva, R.M., 2008. A rapid spectrophotometric determination of persulfate anion in isco. Chemosphere 73 (9), 1540–1543.
Liang, C., Lin, Y.-T., Shih, W.-H., 2009. Treatment of trichloroethylene by adsorption and persulfate oxidation in batch studies. Ind. Eng. Chem. Res. 48 (18), 8373–8380.
Liao, Z., Farrell, J., 2009. Electrochemical oxidation of perfluorobutane sulfonate using boron-doped diamond film electrodes. J. Appl. Electrochem. 39 (10), 1993–1999.
Liu, C., Hatton, J., Arnold, W.A., Simcik, M.F., Pennell, K.D., 2020a. In situ sequestration of perfluoroalkyl substances using polymer-stabilized powdered activated carbon. Environ. Sci. Technol. 54 (11), 6929–6936.
Liu, C., Chu, J., Cápiro, N.L., Fortner, J.D., Pennell, K.D., 2022a. In-situ sequestration of perfluoroalkyl substances using polymer-stabilized ion exchange resin. J. Hazard. Mater. 422, 126960.
Liu, S., Lai, C., Li, B., Liu, X., Zhou, X., Zhang, C., Qin, L., Li, L., Zhang, M., Yi, H., et al., 2022b. Heteroatom doping in metal-free carbonaceous materials for the enhancement of persulfate activation. Chem. Eng. J. 427, 131655.
Liu, Y., Bao, J., Hu, X.-M., Lu, G.-L., Yu, W.-J., Meng, Z.-H., 2020b. Optimization of extraction methods for the analysis of pfoa and pfos in the salty matrices during the wastewater treatment. Microchem. J. 155, 104673.
Lutze, H.V., Brekenfeld, J., Naumov, S., von Sonntag, C., Schmidt, T.C., 2018. Degradation of perfluorinated compounds by sulfate radicals – new mechanistic aspects and economical considerations. Water Res. 129, 509–519.
Maeno, S., Zhu, Q., Sasaki, M., Miyamoto, T., Fukushima, M., 2015. Monopersulfate oxidation of tetrabromobisphenol a by an iron(iii)-phthalocyaninetetrasulfate catalyst coordinated to imidazole functionalized silica particles. J. Mol. Catal. A: Chem. 400, 56–63.
Manz, K.E., Carter, K.E., 2017. Investigating the effects of heat activated persulfate on the degradation of furfural, a component of hydraulic fracturing fluid chemical additives. Chem. Eng. J. 327, 1021–1032.
Manz, K.E., Carter, K.E., 2018. Degradation of hydraulic fracturing additive 2-butoxyethanol using heat activated persulfate in the presence of shale rock. Chemosphere 206, 398–404.
Manz, K.E., Adams, T.J., Carter, K.E., 2018. Furfural degradation through heat-activated persulfate: Impacts of simulated brine and elevated pressures. Chem. Eng. J. 353, 727–735.
Manz, K.E., Palomino, A.M., Cyr, H., Carter, K.E., 2021. Shale particle interactions with organic and inorganic hydraulic fracturing additives. Appl. Geochem. 127, 104901.
Martínez-Mier, E.A., Cury, J.A., Heilman, J.R., Katz, B.P., Levy, S.M., Li, Y., Maguire, A., Margineda, J., O'Mullane, D., Phantumvanit, P., et al., 2011. Development of gold standard ion-selective electrode-based methods for fluoride analysis. Caries Res. 45 (1), 3–12.
Masud, M.A.A., Kim, D.G., Shin, W.S., 2022. Highly efficient degradation of phenolic compounds by fe(ii)-activated dual oxidant (persulfate/calcium peroxide) system. Chemosphere 299, 134392.
Matzek, L.W., Carter, K.E., 2016. Activated persulfate for organic chemical degradation: a review. Chemosphere 151, 178–188.
McCleaf, P., Englund, S., Östlund, A., Lindegren, K., Wiberg, K., Ahrens, L., 2017. Removal efficiency of multiple poly- and perfluoroalkyl substances (pfass) in drinking water using granular activated carbon (gac) and anion exchange (ae) column tests. Water Res. 120, 77–87.
McElroy, A.C., Hyman, M.R., Knappe, D.R.U., 2019. 1,4-dioxane in drinking water: emerging for 40 years and still unregulated. Curr. Opin. Environ. Sci. Health 7, 117–125.
McGregor, R., 2018. In situ treatment of pfas-impacted groundwater using colloidal activated carbon. Remediat. J. 28 (3), 33–41.
McGregor, R., 2020. Six pilot-scale studies evaluating the in situ treatment of pfas in groundwater. Remediat. J. 30 (3), 39–50.
Mitchell, S.M., Ahmad, M., Teel, A.L., Watts, R.J., 2014. Degradation of perfluorooctanoic acid by reactive species generated through catalyzed H_2O_2 propagation reactions. Environ. Sci. Technol. Lett. 1 (1), 117–121.
Patch, D., O'Connor, N., Koch, I., Cresswell, T., Hughes, C., Davies, J.B., Scott, J., O'Carroll, D., Weber, K., 2022. Elucidating degradation mechanisms for a range of per- and polyfluoroalkyl substances (pfas) via controlled irradiation studies. Sci. Total Environ. 832, 154941.
Septian, A., Kumar, A.V.N., Sivasankar, A., Choi, J., Hwang, I., Shin, W.S., 2021. Colloidal activated carbon as a highly efficient bifunctional catalyst for phenol degradation. J. Hazard. Mater. 414, 125474.
Shojaei, M., Kumar, N., Chaobol, S., Wu, K., Crimi, M., Guelfo, J., 2021. Enhanced recovery of per- and polyfluoroalkyl substances (pfass) from impacted soils using heat activated persulfate. Environ. Sci. Technol. 55 (14), 9805–9816.
Simon, J.A., Abrams, S., Bradburne, T., Bryant, D., Burns, M., Cassidy, D., Cherry, J., Chiang, S.-Y., Cox, D., Crimi, M., et al., 2019. Pfas experts symposium: Statements on regulatory policy, chemistry and analytics, toxicology, transport/fate, and remediation for per- and polyfluoroalkyl substances (pfas) contamination issues. Remediat. J. 29 (4), 31–48.
Sühnholz, S., Gawel, A., Kopinke, F.-D., Mackenzie, K., 2021. Evidence of heterogeneous degradation of pfoa by activated persulfate – fes as adsorber and activator. Chem. Eng. J. 423, 130102.
Sun, B., Ma, J., Sedlak, D.L., 2016. Chemisorption of perfluorooctanoic acid on powdered activated carbon initiated by persulfate in aqueous solution. Environ. Sci. Technol. 50 (14), 7618–7624.
Suthersan, S., Quinnan, J., Horst, J., Ross, I., Kalve, E., Bell, C., Pancras, T., 2016. Making strides in the management of "emerging contaminants". Groundw. Monit. Remediat. 36 (1), 15–25.
Szajdzinska-Pietek, E., Gebicki, J.L., 2000. Pulse radiolytic investigation of perfluorinated surfactants in aqueous solutions. Res. Chem. Intermed. 26 (9), 897–912.
Tsitonaki, A., Petri, B., Crimi, M., MosbÆK, H., Siegrist, R.L., Bjerg, P.L., 2010. In situ chemical oxidation of contaminated soil and groundwater using persulfate: a review. Crit. Rev. Environ. Sci. Technol. 40 (1), 55–91.
Tusl, J., 1972. Fluoride ion activity electrode as a suitable means for exact direct determination of urinary fluoride. Anal. Chem. 44 (9), 1693–1694.
Vecitis, C.D., Park, H., Cheng, J., Mader, B.T., Hoffmann, M.R., 2009. Treatment technologies for aqueous perfluorooctanesulfonate (pfos) and perfluorooctanoate (pfoa). Front. Environ. Sci. Eng. 3 (2), 129–151.
Xiao, G., Xu, T., Faheem, M., Xi, Y., Zhou, T., Moryani, H.T., Bao, J., Du, J., 2021. Evolution of singlet oxygen by activating peroxydisulfate and peroxymonosulfate: a review. Int. J. Environ. Res. Public Health 18 (7), 3344.
Xie, M., Tang, J., Kong, L., Lu, W., Natarajan, V., Zhu, F., Zhan, J., 2019. Cobalt doped g-c3n4 activation of peroxymonosulfate for monochlorophenols degradation. Chem. Eng. J. 360, 1213–1222.
Yang, L., He, L., Xue, J., Ma, Y., Xie, Z., Wu, L., Huang, M., Zhang, Z., 2020. Persulfate-based degradation of perfluorooctanoic acid (pfoa) and perfluorooctane sulfonate (pfos) in aqueous solution: review on influences, mechanisms and prospective. J. Hazard. Mater. 393, 122405.
Yang, S., Yang, X., Shao, X., Niu, R., Wang, L., 2011. Activated carbon catalyzed persulfate oxidation of azo dye acid orange 7 at ambient temperature. J. Hazard. Mater. 186 (1), 659–666.
Yao, C., Zhang, Y., Du, M., Du, X., Huang, S., 2019. Insights into the mechanism of non-radical activation of persulfate via activated carbon for the degradation of p-chloroaniline. Chem. Eng. J. 362, 262–268.
Zhang, W., Cao, H., Liang, Y., 2021b. Plant uptake and soil fractionation of five ether-pfas in plant-soil systems. Sci. Total Environ. 771, 144805.
Zhang, H.-C., Han, J.-J., Zhang, X., Guo, P.-C., Xie, D.-H., Sheng, G.-P., 2021a. Undiscovered multiple roles of multivalent cations in the pollutant removal from actual water by persulfate activated by carbon materials. ACS EST Eng. 1 (8), 1227–1235.
Zhao, L., Hou, H., Fujii, A., Hosomi, M., Li, F., 2014. Degradation of 1,4-dioxane in water with heat- and fe2+-activated persulfate oxidation. Environ. Sci. Pollut. Res. 21 (12), 7457–7465.